

See discussions, stats, and author profiles for this publication at: <https://www.researchgate.net/publication/271593221>

Enantioselective Hydroformylation by a Rh-Catalyst Entrapped in a Supramolecular Metallocage

ARTICLE in JOURNAL OF THE AMERICAN CHEMICAL SOCIETY · JANUARY 2015

Impact Factor: 12.11 · DOI: 10.1021/ja512637k · Source: PubMed

CITATIONS

5

READS

153

7 AUTHORS, INCLUDING:



Saeed Raoufmoghaddam

University of Amsterdam

14 PUBLICATIONS 81 CITATIONS

SEE PROFILE



Teodor Parella

Autonomous University of Barcelona

309 PUBLICATIONS 4,649 CITATIONS

SEE PROFILE



Miquel Costas

Universitat de Girona

131 PUBLICATIONS 5,389 CITATIONS

SEE PROFILE



Joost N H Reek

University of Amsterdam

387 PUBLICATIONS 10,831 CITATIONS

SEE PROFILE

Enantioselective Hydroformylation by a Rh-Catalyst Entrapped in a Supramolecular Metallocage

Cristina García-Simón,[†] Rafael Gramage-Doria,[§] Saeed Raoufmoghaddam,[§] Teodor Parella,[‡] Miquel Costas,^{*,†} Xavi Ribas,^{*,†} and Joost N. H. Reek^{*,§}

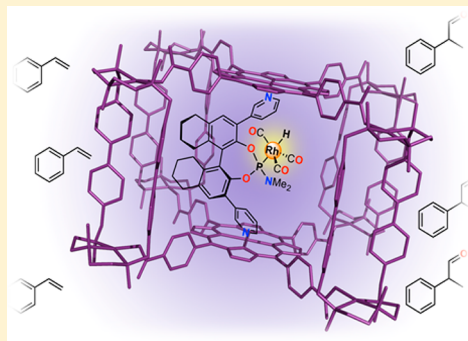
[†]Grup de Química Bioinorgànica i Supramolecular, Institut de Química Computacional i Catàlisi, and Departament de Química, Universitat de Girona. Campus Montilivi, Girona E17071 Catalonia, Spain

[‡]Servei de RMN, Facultat de Ciències, Universitat Autònoma de Barcelona, Campus UAB, Bellaterra E08193 Catalonia, Spain

[§]Homogeneous and Supramolecular Catalysis Group, Van't Hoff Institute for Molecular Science, University of Amsterdam, Science Park 904, 1098 XH Amsterdam, The Netherlands

S Supporting Information

ABSTRACT: Regio- and enantioselective hydroformylation of styrenes is attained upon embedding a chiral Rh complex in a nonchiral supramolecular cage formed from coordination-driven self-assembly of macrocyclic dipalladium complexes and tetracarboxylate zinc porphyrins. The resulting supramolecular catalyst converts styrene derivatives into aldehyde products with much higher chiral induction in comparison to the nonencapsulated Rh catalyst. Spectroscopic analysis shows that encapsulation does not change the electronic properties of the catalyst nor its first coordination sphere. Instead, enhanced enantioselectivity is rationalized by the modification of the second coordination sphere occurring upon catalyst inclusion inside the cage, being one of the few examples in achieving an enantioselective outcome via indirect through-space control of the chirality around the catalyst center. This effect resembles those taking place in enzymatic sites, where structural constraints imposed by the enzyme cavity can impart stereoselectivities that cannot be attained in bulk. These results are a showcase for the future development of asymmetric catalysis by using size-tunable supramolecular capsules.



INTRODUCTION

Reactions taking place at enzyme active sites generally exhibit high rates and exquisite selectivities that differ from those occurring in bulk solution. This is best exemplified in asymmetric catalysis. Weak interactions with amino acid residues precisely modulate the relative orientation of reagents and in some cases assist in their activation.¹ The orientation of the reagents and substrates are controlled by the special environment around the active site leading to highly selective transformations. As such, structural constraints and weak interactions conspire to decrease activation barriers of precise reactions to furnish rapid chemo-, regio-, and stereoselective transformations.^{2–14} Analogous to the spatial constraints imposed by enzyme active sites, metal-based catalysts have been included in molecular nanovessels,^{15–21} with the aim to modulate their activity and selectivity via the second coordination sphere. High chemo- and regioselectivities have been obtained in selected cases, but the number of stereoselective transformations carried out in molecular cages remains scarce.^{2,3,22–28} Furthermore, a common limitation of this kind of supramolecular catalysts is that selectivity is most often increased at the expense of decreasing reaction rates.

A template-ligand approach to form encapsulated ligands and their metal complexes was previously described, and it was

demonstrated that regioselectivity in hydroformylation reactions can be controlled by the second coordination sphere.^{29–32} Generally, this strategy results in exclusively monoligated rhodium complexes that are very reactive. For asymmetric hydroformylation the approach was extended to chiral phosphoramidite,^{10,12} but the monoligated complexes generally resulted in low to moderate enantioselectivity. By using bis-zinc(II)salphen building blocks, the template-ligand approach resulted in the formation of bis-ligated rhodium complexes embedded in a well-defined cavity.¹⁴ Although the enantioselectivity induced by this complex was high, the activity was rather low, especially at room temperature.

Here, we use a different strategy that consists of encapsulating the monophosphoramidite-Rh(I) catalysts^{10–14} in a tetragonal cage that was previously prepared by metal-directed self-assembly.³³ The resulting monoligated catalyst confined within the cavity of the capsule is especially active in the hydroformylation of styrene and derivatives and provides good levels of stereoselectivity. Chiral induction is greatly

Received: December 12, 2014

Revised: January 23, 2015

Accepted: January 29, 2015

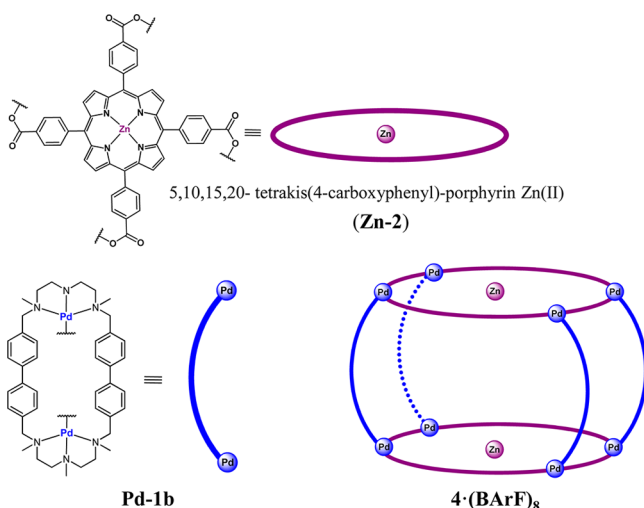
Published: January 29, 2015

enhanced in comparison to the nonencapsulated analogue. These observations provide compelling evidence that the stereoselectivity provided by these catalysts is based on controlling the second coordination sphere by way of the structural constraints imposed by the cage.

RESULTS AND DISCUSSION

Host–Guest Experiments. The synthesis of the tetragonal prismatic nanocage $4\cdot(\text{BARF})_8$ was previously described, showing high affinity for fullerenes from C_{60} to C_{84} .³³ This property has been used in the selective separation of C_{60} from mixtures of fullerenes. Cage $4\cdot(\text{BARF})_8$ is based on two opposing Zn-porphyrin building blocks, linked by four bridging macrocyclic walls that assemble the cage structure through Pd-carboxylate coordination bonds (Scheme 1).

Scheme 1. Schematic Representation of the Building Blocks Used in the Synthesis of Tetragonal-Prismatic Nanocapsule $4\cdot(\text{BARF})_8$



We envisioned that cage $4\cdot(\text{BARF})_8$ would be able to accommodate pyridine-based ligands because of the well-known ability of Zn-porphyrins to interact with pyridine moieties.^{8–14,34} We first sought to prove this by using 4,4'-bipyridine (**4,4'-bpy**) as a guest because we have shown that the Zn...Zn porphyrin distance of $4\cdot(\text{BARF})_8$ can vary from ~ 11 – 14 Å (Scheme 2), owing to the structural flexibility of Pd-carboxylate bonds.³³

As anticipated, UV–vis titration experiments unambiguously indicated an interaction between the nanocapsule and **4,4'-bpy**. High-resolution mass spectrometry (HR-MS) analysis as well as ^1H NMR analysis of the host–guest compound indicated the formation of adduct $4,4'\text{-bpyC}4\cdot(\text{BARF})_8$ in a 1:1 stoichiometry (Experimental Section and Figures S1–4).

The geometry of adduct $4,4'\text{-bpyC}4\cdot(\text{BARF})_8$ was fully characterized by means of 1D and 2D NMR spectroscopy (Figures S5–8). At room temperature, the ^1H NMR spectrum exhibited some moderate upfield shifts in the signals, corresponding to some of the aromatic protons of the cage. Additionally, an isolated strongly upfield-shifted doublet signal was observed, centered at 4.91 ppm and corresponding to **4,4'-bpy** (Figure S5a). 2D COSY and ^1H – ^{13}C HSQC spectra confirmed that the **4,4'-bpy** signals (resonating at 4.91/120.4 and 2.19/142.2 $^1\text{H}/^{13}\text{C}$ ppm) experience a strong upfield-chemical-shift effect upon encapsulation, caused by the

anisotropic ring currents from the porphyrin moieties. The stronger effect on proton **a** is a consequence of its very close proximity to the aromatic rings of the porphyrin (Figure 1a). The **4,4'-bpy** nitrogen chemical shift was also expected to be a good indicator of encapsulation because it will also be altered by the porphyrin rings' electron density.^{35,36} Therefore, ^1H – ^{15}N HMBC spectra of free and encapsulated **4,4'-bpy** were recorded. A chemical shift from 319.5 (**4,4'-bpy**) to 274.6 ppm ($4,4'\text{-bpyC}4\cdot(\text{BARF})_8$) further confirmed the coordination of the N atoms from bpy to the Zn(II)-porphyrins (Figure S7–8). DOSY-2D NMR experiments also supported the formation of the $4,4'\text{-bpyC}4\cdot(\text{BARF})_8$ 1:1 host–guest adduct (Supporting Information, Section 1.4 and Figure S9).

The next step was the inclusion of phosphoramidite (**S**)- α within $4\cdot(\text{BARF})_8$ cage with the aim of preparing in situ the encapsulated Rh-catalysts to be then employed in asymmetric hydroformylation reactions. We envisioned that the $\text{N}_{\text{pyr}}\cdots\text{N}_{\text{pyr}}$ distance in α (~ 11 Å) might be suitable to fit inside $4\cdot(\text{BARF})_8$, whereas ligand β (containing pyridine groups in the para positions) does not have a suitable orientation to bind simultaneously with both pyridyl groups to the porphyrin units of the cage. UV–vis titration between capsule $4\cdot(\text{BARF})_8$ and ligand α displayed a bathochromic shift of the Soret band from the porphyrins, exhibiting two isosbestic points, suggesting the formation of a 1:1 host–guest adduct (Figure 2a,b). The 1:1 interaction was further confirmed by Job's plot analysis (Figure 2c). From the UV–vis data, a binding constant of $(3.6 \pm 0.2) \times 10^6 \text{ M}^{-1}$ was obtained. This high binding constant can be illustratively compared to that observed for $\alpha(\text{Zn-TPP})_2$ (K_a ca. 10^3 M^{-1}), strongly suggesting that α is indeed bound in a ditopic fashion within $\alpha\text{C}4\cdot(\text{BARF})_8$.¹⁰ As a consequence, the phosphoramidite ligand is located in the middle of the supramolecular cage. HRMS experiments also supported the formation of $\alpha\text{C}4\cdot(\text{BARF})_8$ (Figure S10). As anticipated, ligand β is not encapsulated within nanocapsule $4\cdot(\text{BARF})_8$, as shown by UV–vis studies (Figure S11).

^1H NMR characterization of $\alpha\text{C}4\cdot(\text{BARF})_8$ displayed trends similar to those of $4,4'\text{-bpyC}4\cdot(\text{BARF})_8$ (Figures S12–17). The ^1H NMR spectrum of adduct $\alpha\text{C}4\cdot(\text{BARF})_8$ in acetonitrile at 298 K exhibited some line-broadening effects for all BARF[−] signals, whereas smaller and very broad signals were observed for the encapsulated ligand (between 5 and 6.5 ppm) and the capsule. The broad signals might illustrate some complex dynamic process and loss of symmetry of the host–guest adduct in comparison with the highly symmetric structure of empty $4\cdot(\text{BARF})_8$. In addition, a broad upfield-shifted signal was observed at -0.3 ppm. To simplify the spectrum, it was recorded at 243 K. In the latter spectrum, the signals became sharper and suitable for study by 2D NMR methods. 2D COSY, NOESY, and HSQC spectra recorded at 243 K allowed us to identify and assign most of the signals belonging to encapsulated ligand α (Figure 1b). Compared to the free ligand, all ^1H signals corresponding to confined α appeared doubled at 243 K, confirming that the ligand is not symmetric when bound to the nanocage. Moreover, very pronounced upfield effects are observed for all pyridine aromatic protons from ligand α (resonating around 1–2 ppm), in strong agreement with the trends observed for model substrate **4,4'-bpy**. The three-spin proton systems belonging to the pyridine rings of α (protons labeled as 1, 1', 2, 2', 3, 3', 5, 5', 8, and 8'; Figures 1b and S15) were quickly assigned from the evident COSY and NOE cross-peaks, and their ^{13}C chemical shifts were assigned by HSQC. Protons 8 and 8', which appeared as two

Scheme 2. Zn^{II}-Template (Zn-TPP) and Mono-Phosphoramidite Ligands (α , β , γ , δ) Used in This Study as Well as the Structure of Host–Guest α C4·(BARF)₈ Cage Structure and Ligand-Template Systems α (Zn-TPP)₂ and β (Zn-TPP)₂

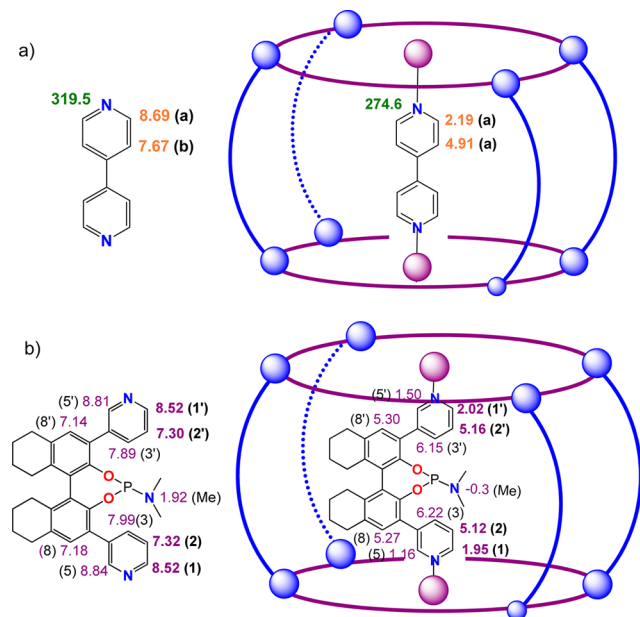
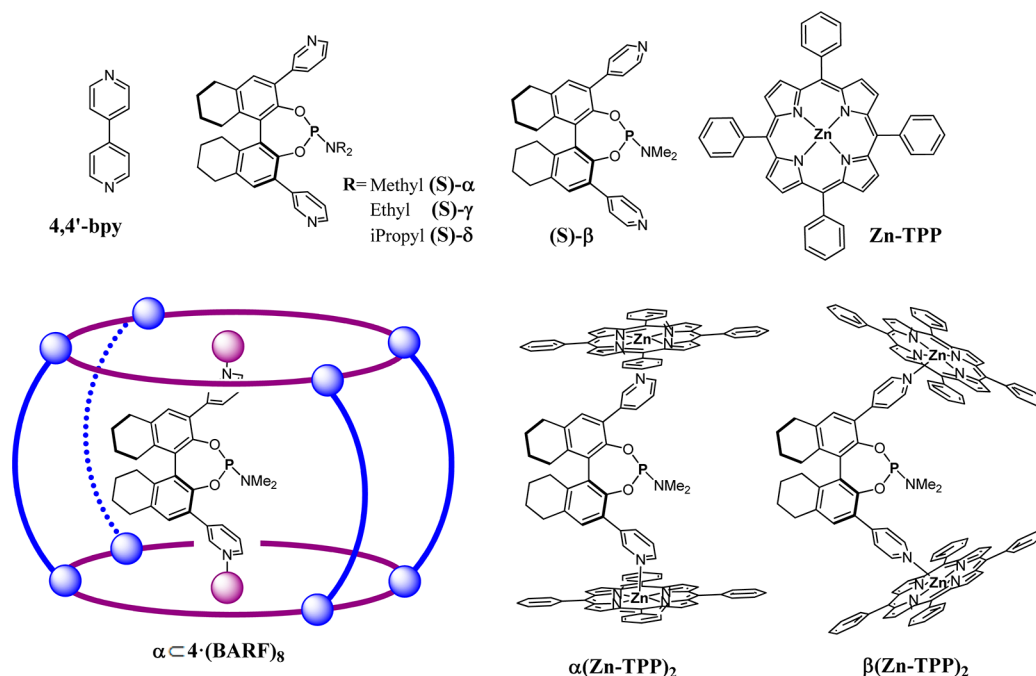


Figure 1. (a) ¹H and ¹⁵N NMR assignment of free and encapsulated 4,4'-bpy (experiments were carried out in CD₃CN at 298 K). (b) ¹H NMR assignment of free and encapsulated ligand α (experiments were carried out in CD₃CN at 298 and 243 K respectively). The corresponding spectra are included in the Supporting Information.

separated singlets at 5.30 and 5.27 ppm, were assigned by NOE enhancement, with the aromatic proton resonating at 1.50/1.16 ppm, respectively. The *N*-methyl signals were assigned to the signal at −0.3 ppm, on the basis of the NOEs, with the surrounding protons observed in the NOESY spectrum (Figure S16).

Interestingly, the ³¹P NMR data exhibited a singlet at \approx 137.0 ppm, similar to that of free ligand α , indicating that the phosphorus is not coordinated to any of the metals of 4-

(BARF)₈ and therefore remains available for coordination to the rhodium metal center that is used for catalysis (Figure S18).

The sum of the spectroscopic data led to the conclusion that α is encapsulated and is strongly bound to 4·(BARF)₈. Furthermore, this binding did not involve the phosphine atom, which remains available for binding the rhodium metal.

Preparation of the Encapsulated Catalyst. Rh(I) catalyst was formed in situ by addition of 1 equiv of [Rh(acac)(CO)₂] to a deuterated toluene/acetonitrile (5:2 v/v)⁶ solution of α C4·(BARF)₈ (Scheme 3). Key features of the rhodium complex have been identified by IR and NMR spectroscopy (Figures S19–20). The carbonyl vibration of the CO ligand was detected by IR spectroscopy (ν = 1995 cm^{−1}, Figure S21). The ³¹P NMR displays a typical doublet centered at δ = 147 ppm, with a phosphorus–rhodium coupling (¹*J*_{P–Rh} = 260 Hz), suggesting the formation of monoligated species (Scheme 3).¹⁰

Under catalytic conditions (5 bar of H₂/CO, 1:1), the rhodium acac precursor was converted into the typical hydride species; in this case, [trans-Rh(H)(CO)₃· α C4·(BARF)₈] was observed. The high-pressure (HP) ¹H NMR spectrum of [Rh(H)(CO)₃· α C4·(BARF)₈] shows signals corresponding to the catalyst–capsule adduct (Figure S22), thus indicating its stability under the catalytic conditions. Moreover, a double doublet centered at −11.7 ppm is observed, indicating formation of the hydride at a monoligated rhodium complex (Scheme 3). The large phosphorus coupling (*J*_{H–P} = 175.5 Hz) shows that the phosphorus donor atom is located trans to the hydride, similar to that observed for [trans-Rh(H)(CO)₃· β (Zn-TPP)₂].^{10,11} The ¹H-³¹P-NMR spectrum displays a single peak at −11.9 ppm, confirming that the large coupling is between the phosphorus and the hydride (Figure S22–S23).

Application of the Encapsulated Catalyst in Asymmetric Hydroformylation Catalysis. Once the encapsulated Rh catalyst was thoroughly characterized, we focused on the investigation of its catalytic performance in the asymmetric

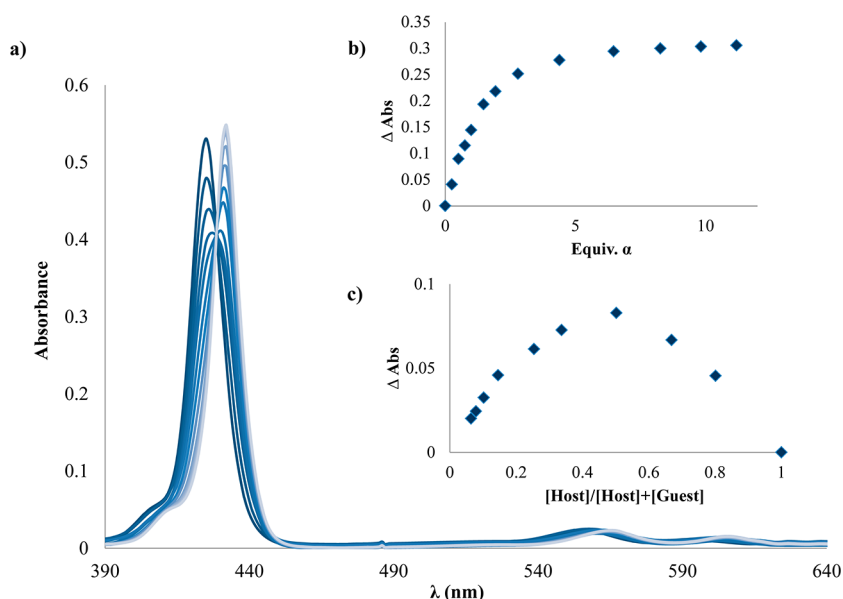
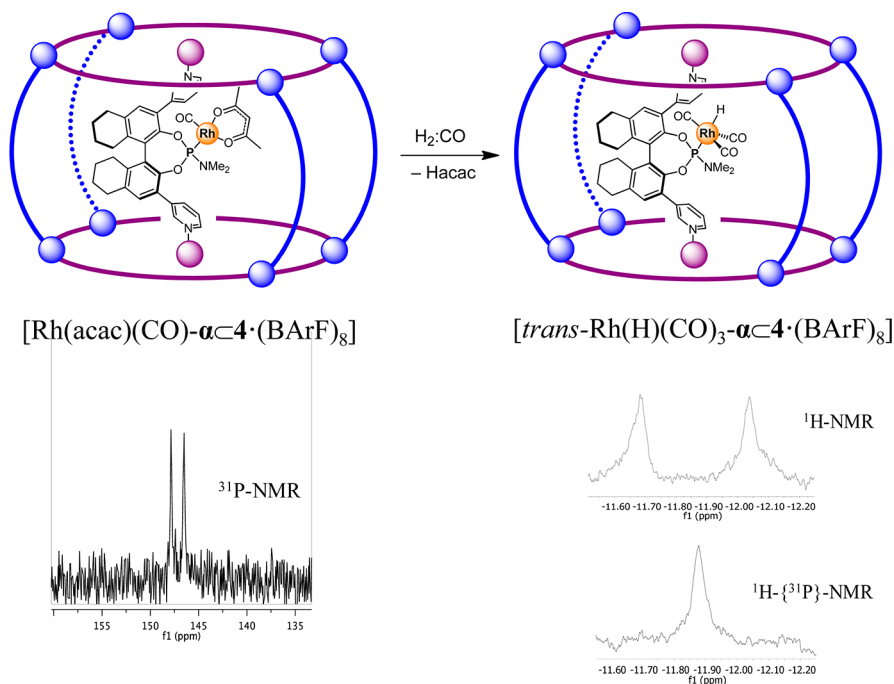


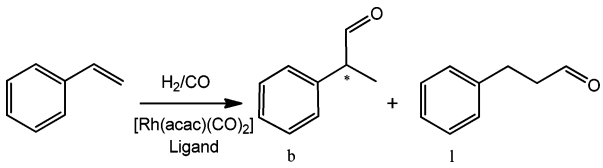
Figure 2. (a) UV-vis monitoring of the titration of 4·(BArF)₈ nanocapsule with ligand α, at a fixed total concentration (4.32×10^{-7} M) of nanocapsule 4·(BArF)₈ in a toluene/CH₃CN mixture (9:1). (b) Absorbance variation at the Soret band versus different concentrations of the ligand. (c) Job's plot showing a 1:1 stoichiometry for the host-guest complex of nanocage 4·(BArF)₈ and ligand α.

Scheme 3. NMR and High-Pressure NMR Spectra of [Rh(acac)(CO)-αC4·(BArF)₈] and [trans-Rh(H)(CO)₃-αC4·(BArF)₈]



hydroformylation (AHF) of styrene.^{37–41} To clearly study the effect of encapsulation, catalytic activities of [Rh(acac)(CO)-αC4·(BArF)₈] were compared with that of the Rh-complex of α(Zn-TPP)₂. Because of limited solubility, catalyst loading was kept low (2×10^{-4} mol %). As is common practice, a 5-fold excess of ligand/capsule (αC4·(BArF)₈) was used in all the experiments in order to avoid the formation of ligand-free rhodium species, an active and nonselective catalyst that could compromise the selectivity. Reactions were carried out at room temperature, and the turnover numbers (TON) and enantiomeric excesses (ee) are reported in Tables 1–4.

Much to our delight, encapsulated Rh catalyst [Rh(H)-(CO)₃-αC4·(BArF)₈] gave a higher turnover number (Table 1, entries 1, 6, and 7) than the nonencapsulated analogue (Table 1, entries 3 and 9) and the catalyst based on assembled α(ZnTPP)₂ (Table 1, entries 4 and 10). As previously observed, when the reaction is carried out with rhodium complex α in the absence of zinc(II) porphyrins, very low conversion is observed, which is likely due to the presence of free pyridyl groups that compete with the substrate for coordination at the rhodium center. The effect of encapsulation on the selectivity of the reaction was remarkable: when assembled α(Zn-TPP)₂ was used as ligand, a modest 9% ee was

Table 1. Asymmetric Hydroformylation of Styrene Using Rh-Catalysts Based on α C4·(BArF)₈ Cage Structure and Ligand-Template System α (Zn-TPP)₂^a


entry	ligand	b/l ^d	ee (%) ^e	conv (%)	TON
1	α C4·(BArF) ₈	99:1	74 (R)	14	797
2		n.d. ^f	n.d. ^f	<1	<1
3	α	99:1	<1	6	342
4	α (ZnTPP) ₂	99:1	9(R)	7	363
5	4·(BArF) ₈	99:1	<1	6	300
6 ^b	α C4·(BArF) ₈	99:1	65 (R)	32	1600
7 ^c	α C4·(BArF) ₈	99:1	70 (R)	7	339
8 ^c		n.d. ^f	n.d. ^f	<1	<1
9 ^c	α	99:1	8 (R)	4	197
10 ^c	α (ZnTPP) ₂	99:1	16 (R)	4	215
11	γ C4·(BArF) ₈	99:1	79 (R)	6	308
12	γ	99:1	7 (R)	3	136
13	δ C4·(BArF) ₈	99:1	77 (R)	2	104
14	δ	99:1	6 (R)	1	41

^aReagents and conditions: [Rh] = 33 μ M in toluene/MeCN (4:1), ligand/capsule/[Rh(acac)(CO)₂] = 5, alkene/rhodium = 5000, rt, 20 bar, 96 h. Rh complex: [Rh(acac)(CO)₂]. ^bThe catalytically active species is generated under 20 bar of syngas, 16 h, 40 °C. Then the styrene was added and the reaction was carried out at rt, 20 bar, 96 h. ^c[Rh] = 33 μ M in toluene/MeCN (2:3), rt, 20 bar, 96 h. ^dRatio of branched and linear aldehyde. ^eEnantiomeric ratio determined by chiral GC analysis (Supelco BETA DEX 225). ^fn.d. = nondetected.

observed, whereas complete encapsulation of the ligand via α C4·(BArF)₈ resulted in 74% ee (Table 1, entries 1–4). The encapsulated catalyst gives among the highest chemo- and stereoselectivities for a monoligated rhodium complex reported so far.⁶ Using an incubation period at 40 °C before initiating the reaction resulted in a higher TON, at the expense of the selectivity (TON increased from 797 to 1600, enantiomeric excess decreased from 74 to 65%; Table 1, entries 1 and 6). Further optimization by changing the toluene/acetonitrile ratio did not improve the results (Table 1, entries 7–10). A control experiment in which capsule 4·(BArF)₈ and the Rh complex were used as catalyst provided racemic aldehyde (Table 1, entry 5). Moreover, ¹H NMR experiments were carried out in order to see if the nanocapsule still maintains its structure under the high-pressure reaction conditions employed in catalytic experiments. Effectively, the cage remains unaltered even after heating a solution of 4·(BArF)₈ at 60 °C under 5 bar of syngas for 2 h (Figure S24). No precipitate appeared on the NMR tube, strongly suggesting that the capsule is not destroyed under these conditions, likely because the capsule's building blocks are not soluble in DCM. Cage decomposition would have led to the appearance of a precipitate. As a complementary experiment, the crude reaction mixture obtained in one of the catalytic experiments was dried and redissolved in a toluene-*d*₈/CD₃CN mixture to record the ¹H NMR. The spectrum showed that the integrity of the ligand–cage adduct was still maintained after catalysis (Figure S25).

To fine-tune the supramolecular assemblies and to optimize the activity and the selectivity of the catalytic transformation, the Rh-catalyzed AHF of styrene was further studied using

ligands γ (R = Et) and δ (R = *i*-Pr) in the presence and the absence of cage 4·(BArF)₈ (Scheme 1 and Table 1, entries 11–14). Replacing ligand α for γ leads to a slight increase in the enantiomeric excess (from 74 to 79%) at the expense of activity (TON decreases from 797 to 308). When using ligand δ , a small increase in the enantiomeric excess was also observed (from 74 to 77%), but the activity was drastically lower in comparison with ligand α C4·(BArF)₈ (TON decreases from 797 to 104). These results reveal that small modifications to the ligand building block allow optimization of the selectivity and activity of the supramolecular catalysts, which opens the door to future catalyst optimization. So far, of this new class of encapsulated catalysts, α C4·(BArF)₈ affords the best compromise in enantiomeric excess and TON for the AHF of styrene.

Preliminary molecular modeling studies were carried out (Figures S26–29) to shine light on the effect of encapsulation on the performance of the Rh catalyst. For the nonencapsulated catalysts (Rh(H)(CO)₃– α), calculations show that there is a wide space for coordination of the styrene molecule in four orientations to the two available coordination sites. These will lead to subsequent selectivity in determining hydride migration, which constitutes the key step that determines enantioselectivity. Because the substrate can approach the catalyst with multiple orientations, the overall stereoselectivity that results when reactions are carried out in the absence of the cage is poor. In contrast, when the catalyst is docked into the nanocapsule, the cage walls prevent most of the coordination modes of styrene to the Rh center, effectively blocking some of the reaction pathways (Figures S28–29).

Given the promising results obtained in the AHF of styrene, the substrate scope of α C4·(BArF)₈ was evaluated using different para-R-substituted styrene derivatives (R = H, Cl, CH₃, OCH₃, and *t*-Bu). The results obtained for these substrates were similar to the ones obtained for styrene (Table 2); in all cases, the best activities were obtained when ligand α was encapsulated in cage α C4·(BArF)₈. The conversion (TON) and the regioselectivity depended to some extent on the substituent on the styrene. Selectivity toward the branched aldehyde was maintained when R = *t*-Bu (Table 2, entry 17); whereas for R = CH₃ and OCH₃, the b/l ratio was slightly lower (91:9; Table 2, entries 9 and 13). For 4-Cl-styrene, the selectivity decreased even further to b/l = 80:20 (Table 2, entry 5). In all cases, substrates bearing substituents at position 4 showed a decrease in enantiomeric excess. Nevertheless, comparison of these results with those of rhodium catalyst α (Zn-TPP)₂ consistently showed the benefits of catalyst encapsulation in cage 4·(BArF)₈. In general, enantiomeric excesses are below 12% for α (Zn-TPP)₂ (Table 2, entries 4, 8, 12, 16) but are over 58% for the encapsulated catalyst. For the most bulky substrate, when R = *t*-Bu, the effect is less pronounced because the enantiomeric excess improves from a moderate value of 31 to 48% (Table 2, entries 17 and 20).

The substrate scope was further extended to ortho-, meta- and para-substituted methoxystyrene derivatives, in order to investigate the effect of steric interactions in more detail. Higher TON and enantiomeric excess values were obtained for *p*-methoxystyrene when α C4·(BArF)₈ was used as catalyst (Table 3, entry 1), compared to the complex based on α (Zn-TPP)₂ (Table 3, entry 4). In contrast, for *o*-methoxystyrene, the caged catalyst gave much lower TON than the complex based on α (Zn-TPP)₂ (Table 3, entry 9 vs 12). Because *ortho*- and *para*-methoxystyrene can be considered to have electroni-

Table 2. Asymmetric Hydroformylation of Styrene Derivatives Using Rh-Catalysts Based on $\alpha\text{C4}(\text{BArF})_8$ Cage Structure and Ligand-Template System $\alpha(\text{Zn-TPP})_2$ ^a

entry	R	catalyst	b/l ^b	ee (%) ^c	conv (%)	TON
1	H	$\alpha\text{C4}(\text{BArF})_8$	99:1	74 (R)	14	797
2	H		n.d. ^d	n.d. ^d	<1	<1
3	H	α	99:1	<1	6	342
4	H	$\alpha(\text{Zn-TPP})_2$	99:1	9 (R)	7	363
5	Cl	$\alpha\text{C4}(\text{BArF})_8$	80:20	58 (R)	14	761
6	Cl		n.d. ^d	n.d. ^d	<1	<1
7	Cl	α	91:9	<1	4	180
8	Cl	$\alpha(\text{Zn-TPP})_2$	91:9	11 (R)	12	577
9	CH ₃	$\alpha\text{C4}(\text{BArF})_8$	91:1	61 (R)	31	1564
10	CH ₃		n.d. ^d	n.d. ^d	<1	<1
11	CH ₃	α	91:9	<1	3	140
12	CH ₃	$\alpha(\text{Zn-TPP})_2$	91:9	12 (R)	10	482
13	OCH ₃	$\alpha\text{C4}(\text{BArF})_8$	91:9	69 (R)	22	1125
14	OCH ₃		99:1	<1	4	180
15	OCH ₃	α	99:1	<1	3	168
16	OCH ₃	$\alpha(\text{Zn-TPP})_2$	97:3	<1	7	340
17	<i>t</i> -Bu	$\alpha\text{C4}(\text{BArF})_8$	99:1	48 (R)	21	1042
18	<i>t</i> -Bu		99:1	<1	2	107
19	<i>t</i> -Bu	α	99:1	<1	4	180
20	<i>t</i> -Bu	$\alpha(\text{Zn-TPP})_2$	97:3	31 (R)	7	361

^aReagents and conditions: [Rh] = 33 μM in toluene/MeCN (4:1), ligandCcapsule/[Rh(acac)(CO)₂] = 5, alkene/rhodium = 5000, rt, 20 bar, 96 h. Rh complex: [Rh(acac)(CO)₂]. ^bRatio of branched and linear aldehyde. ^cEnantiomeric ratio determined by chiral GC analysis (Supelco BETA DEX 225). ^dn.d. = nondetected

Table 3. Asymmetric Hydroformylation of *p*-, *m*-, and *o*-Methoxystyrene Using Rh-Catalysts Based on $\alpha\text{C4}(\text{BArF})_8$ Cage Structure and Ligand-Template System $\alpha(\text{Zn-TPP})_2$ ^a

entry	ligand	b/l ^b	ee (%) ^c	conv (%)	TON
<i>para</i> -Methoxystyrene					
1	$\alpha\text{C4}(\text{BArF})_8$	91:9	69(R)	22	1125
2		99:1	<1	4	180
3	α	99:1	<1	3	168
4	$\alpha(\text{Zn-TPP})_2$	97:3	<1	7	340
<i>meta</i> -Methoxystyrene					
5	$\alpha\text{C4}(\text{BArF})_8$	99:1	56	10	519
6		n.d. ^d	n.d. ^d	<1	<1
7	α	99:1	<1	2	113
8	$\alpha(\text{Zn-TPP})_2$	99:1	<1	4	180
<i>ortho</i> -Methoxystyrene					
9	$\alpha\text{C4}(\text{BArF})_8$	99:1	47	2	127
10		n.d. ^d	n.d. ^d	<1	<1
11	α	99:1	<1	2	109
12	$\alpha(\text{Zn-TPP})_2$	99:1	<1	5	245

^aReagents and conditions: [Rh] = 0.033 mM in toluene/MeCN (4:1), ligandCcapsule/[Rh(acac)(CO)₂] = 5, alkene/rhodium = 5000, rt, 20 bar, 96 h. Rh complex: [Rh(acac)(CO)₂]. ^bRatio of branched and linear aldehyde. ^cEnantiomeric ratio determined by chiral GC analysis (Supelco BETA DEX 225). ^dn.d. = nondetected.

cally equivalent olefinic sites, the sharp difference is fully attributed to the structural discrimination imposed by cage 4-

(BArF)₈. For *m*-methoxystyrene, the encapsulated catalyst gave rise to a higher TON (519) than the control reaction carried out with $\alpha(\text{Zn-TPP})_2$ template, and the product was formed with 56% ee (Table 3, entry 5). Most importantly, for *p*- and *m*-methoxystyrene, the selectivity obtained with the caged catalyst was much higher than that obtained with the catalyst based on $\alpha(\text{Zn-TPP})_2$ (Table 3, entries 4 and 8), which again clearly substantiates the importance of catalyst confinement in the AHF of styrene.

Finally, we carried out AHF catalysis of styrene at variable concentrations of $\alpha\text{C4}(\text{BArF})_8$ and $\alpha(\text{Zn-TPP})_2$. We reasoned that the relatively high association constant of the ligand in the cage (i.e., stability constant) of $\alpha\text{C4}(\text{BArF})_8$ compared to $\alpha(\text{Zn-TPP})_2$ should translate to a higher concentration window in which these supramolecular catalysts can operate. As such, we carried out experiments at four catalyst concentrations ranging from 147 to 1 μM (Table 4). Upon lowering the

Table 4. Asymmetric Hydroformylation of Styrene at Different Rh-Catalyst Concentrations^a

entry	catalyst	[Rh] (μM)	b/l ^b	ee (%) ^c	conv (%)	TON
1	$\alpha\text{C4}(\text{BArF})_8$		98:2	71	97	193
2			96:4	<1	64	128
3	α	147	98:2	3	90	180
4	$\alpha(\text{Zn-TPP})_2$		97:3	15	92	183
5	$\alpha\text{C4}(\text{BArF})_8$		97:3	68	79	158
6			91:9	<1	20	39
7	α	33	97:3	3	88	176
8	$\alpha(\text{Zn-TPP})_2$		97:3	16	49	99
9	$\alpha\text{C4}(\text{BArF})_8$		99:1	74	14	29
10				n.d. ^d	0	0
11	α	6	99:1	<1	17	33
12	$\alpha(\text{Zn-TPP})_2$		99:1	<1	15	31
13	$\alpha\text{C4}(\text{BArF})_8$			n.d. ^d	0	0
14				n.d. ^d	0	0
15	α	1		n.d. ^d	0	0
16	$\alpha(\text{Zn-TPP})_2$			n.d. ^d	0	0

^aReagents and conditions: toluene/MeCN (4:1), ligandCcapsule/[Rh(acac)(CO)₂] = 5, alkene/rhodium = 200, rt, 20 bar, 96 h. Rh complex: [Rh(acac)(CO)₂]. ^bRatio of branched and linear aldehyde. ^cEnantiomeric ratio determined by chiral GC analysis (Supelco BETA DEX 225). ^dn.d. = nondetected.

concentration of Rh- $\alpha\text{C4}(\text{BArF})_8$, the TON is lower (as expected) because of the typical positive order of the catalyst concentration on the reaction rate. Most indicative of the stability of the assembly is the selectivity. The selectivity induced by the encapsulated catalysts remains high (71 \pm 3% ee) even at concentrations of 6 μM , indicating that under these conditions catalysis is still dominated by the encapsulated catalyst (Figure S30). In contrast, when catalyst Rh- $\alpha(\text{Zn-TPP})_2$ was used at 6 μM , the product was formed in racemic form, and the TON was also similar to that of the control experiment where no porphyrins were present. These results are in agreement with the significantly more robust nature of catalyst $\alpha\text{C4}(\text{BArF})_8$ compared to $\alpha(\text{Zn-TPP})_2$.

CONCLUSIONS

This work describes the encapsulation of a monoligated chiral rhodium complex in a self-assembled molecular cage. Encapsulated catalyst Rh- $\alpha\text{C4}(\text{BArF})_8$ exhibits the highest selectivities in the asymmetric hydroformylation of styrenes

among monoligated rhodium catalysts.⁶ Most significantly, the stereoselectivity observed in the hydroformylation of styrenes upon encapsulation of the catalyst is substantially improved with regard to analogous reactions carried out with the catalyst operating in bulk solution. Therefore, the cage can be considered as a second coordination sphere of the catalyst, reminiscent of enzymatic active sites. On the basis of these observations, we envision that the use of the second-coordination-sphere tuning strategy over the selectivity of catalytic events may be more broadly applicable. The size-tunability of cage 4-(BARF)₈, the high affinity for pyridine-containing ligands, and the possibility of modifying the apertures of the cage all provide strong fundamentals for the future development of these cage structures for asymmetric catalysis.

EXPERIMENTAL SECTION

Materials. Unless indicated otherwise, the reagents and solvents used were commercially available reagent-quality, and reactions were carried out under an atmosphere of nitrogen using standard Schlenk techniques. Ligands **α**¹⁴ and **β**¹⁰ and molecular cage 4-(BARF)₈³³ were synthesized following previously reported procedures.

Physical Methods. NMR spectra (¹H, ³¹P, and ¹³C) were measured on Bruker DRX 400 MHz, Bruker AVANCE 500 MHz, Bruker AVANCE 600 MHz, and Varian Inova 500 MHz spectrometers; CDCl₃, CD₃CN, or toluene-*d*₈ were used as solvents, unless further indicated. HRMS data were obtained on a Bruker MicroTOF-Q-II apparatus, using acetonitrile as the mobile phase. UV–vis spectroscopy was carried out on an Agilent 8452 UV–vis spectrophotometer with a 1 cm quartz cell. Gas chromatographic analyses were run on a Shimadzu GC-17A apparatus (split/splitless injector, J&W 30 m column, film thickness = 3.0 μm, carrier gas 70 kPa He, FID Detector). Chiral GC separations were conducted on an Iterscience HR GC apparatus with a Supelco β-dex 225 capillary column. IR experiments were carried out at room temperature on a Nicolet 510 FTIR spectrometer. Molecular modeling calculations were carried out using PM3-Spartan molecular modeling program.

Synthesis of Ligands **γ and **δ**.** In a flame-dried Schlenk flask, 200 mg (0.44 mmol) of **d**, pyridine (0.068 mL, 0.88 mmol), and DMAP (10 mol %) were suspended in dry toluene (4.4 mL, 0.1 M). The solution was cooled to 0 °C, and distilled PCl₃ (0.080 mL, 0.88 mmol) was added dropwise over 10 min. The mixture was warmed to room temperature and then refluxed overnight. The reaction mixture was cooled to room temperature, and the formation of product was checked by ³¹P NMR. The solvent and the residual PCl₃ were removed in vacuum. The resulting solid was used for the next step without any further purification.

In a flame-dried Schlenk flask, dialkylamine (0.44 mmol) and pyridine (0.040 mL, 0.48 mmol) were dissolved in dry toluene (1 mL). The solution was added dropwise to a cooled (0 °C) mixture of **e** (225.7 mg, 0.44 mmol) in dry toluene (5 mL). The mixture was warmed to room temperature and stirred overnight at room temperature. The precipitate formed was filtered over a pad of Celite under argon, and the solvent was evaporated in vacuum to obtain **α**, **γ**, and **δ**.

The reaction scheme (including representations **a–e**) is shown in the Supporting Information; see also Figures S31 and 32.

Ligand **γ.** Yield: 81% (white foam); ¹H NMR (400 MHz, CDCl₃): δ = 8.85 (m, 2H), 8.54 (dd, 2H), 7.96 (dt, 1H), 7.90 (dt, 1H), 7.28 (m, 2H), 7.16 (s, 1H), 7.14 (s, 1H), 2.90 (m, 4H), 2.54 (m, 2H), 2.35 (m, 4H), 1.87 (m, 8H), 0.51–0.59 (t, 6H); ¹³C NMR: 150.2, 149.1, 147.2, 138.0, 136.2, 130.2, 129.1, 128.4, 122.5, 122.1, 34.2, 30.2, 29.1, 28.3, 27.8, 23.1, 22.2; ³¹P NMR: δ = 140.85 ppm.

Ligand **δ.** Yield: 52% (white foam); ¹H NMR (400 MHz, Toluene): δ = 8.99–9.07 (dd, 2H), 8.43 (d, 2H), 7.84 (dt, 1H), 7.73 (dt, 1H), 7.01 (m, 2H), 6.97 (s, 1H), 6.71 (s, 1H), 2.68 (m, 6H), 2.44 (m, 2H), 1.79 (m, 2H), 1.59 (m, 8H), 0.87 (4*d, 12H); ¹³C NMR: 153.2, 152.7, 150.2, 14.1, 139.2, 138.0, 135.2, 130.2, 129.1,

128.6, 122.1, 47.5, 46.6, 35.6, 34.2, 31.1, 28.3, 12.8, 12.1, 11.2; ³¹P NMR: δ = 139.89 ppm.

Preparation of 4,4'-bpyC4-(BARF)₈.³³ 4.0 mg of 4-(BARF)₈ nanocapsule (0.33 μmols, 1 equiv) was dissolved in 100 μL of CH₃CN. Then, 1 equiv of 4,4'-bpy dissolved in 400 μL of toluene was added. The mixture was stirred at room temperature for 5 min. After the reaction time, the mixture was filtered through cotton and recrystallized by diethyl ether diffusion. A quantitative yield was obtained. ¹H NMR (400 MHz, CD₃CN) δ ppm: 8.59 (s, 16 H, pyrrole ring), 8.58 (dd, 8 H, arom-porph), 8.34 (dd, *J* = 8 Hz, 8 H, arom-porph), 8.28 (d, *J* = 8.5 Hz, 32 H, arom-clip), 8.13 (m, 32 H arom-clip + 8 H arom-porph), 7.99 (dd, *J* = 8 Hz, 8 H, arom-porph), 7.67 (m, 96 H, NaBARF)*, 4.95 (m, 4 H, bpy), 4.04 (d, *J* = 13 Hz, 16 H, –CH₂–), 3.73 (m, 16 H, –CH₂–), 3.60 (s, 48 H, N–CH₃), 3.37 (m, 16 H, –CH₂–), 3.14 (d, *J* = 13 Hz, 16 H, –CH₂–), 2.48 (dd, *J* = 13.5, 16 H, –CH₂–), 2.38 (dd, *J* = 13.5, 16 H, –CH₂–), 1.59 (s, 24 H, N–CH₃). HRMS (*m/z*): Calcd 2186.923, Found 2186.910 ({4,4'-bpyC4-(BARF)₄}⁴⁺); Calcd 1577.118, Found 1577.115 ({4,4'-bpyC4-(BARF)₃}⁵⁺); Calcd 1170.251, Found 1170.255 ({4,4'-bpyC4-(BARF)₂}⁶⁺); Calcd 879.634, Found 879.637 ({4,4'-bpyC4-(BARF)}⁷⁺); Calcd 661.796, Found 661.799 ({4,4'-bpyC4-(BARF)}⁸⁺).

Preparation of αC4-(BARF)₈. 9 mg of 4-(BARF)₈ nanocapsules (0.33 μmols, 1 equiv) was dissolved in 300 μL of CH₃CN. Then, 1 equiv of **α** dissolved in 1200 μL toluene was added. The mixture was stirred at room temperature for 5 min. After the reaction time, the mixture was filtered through cotton and recrystallized by diethyl ether diffusion. A quantitative yield was obtained. HRMS (*m/z*): Calcd 2278.453, Found 2278.452 ({αC4-(BARF)₄}⁴⁺); Calcd 1650.120, Found 1650.151 ({αC4-(BARF)₃}⁵⁺); Calcd 1231.231, Found 1231.283 ({αC4-(BARF)₂}⁶⁺); Calcd 931.942, Found 931.945 ({αC4-(BARF)}⁷⁺); Calcd 707.621, Found 707.693 ({αC4-(BARF)}⁸⁺).

Preparation of trans-[Rh(H)(CO)₃-α]C4-(BARF)₈ Complex for High-Pressure NMR Experiment. To 16 mg of 4-(BARF)₈ (0.0013 μmol) was added 1 equiv of the phosphoramidite ligand (**α**, **β**, **γ**, or **δ**) and 1 equiv of Rh(acac)(CO)₂ in a 7:3 (v/v) mixture of *d*₈-toluene/CD₃CN (1.2 mL). The mixture was transferred into a 5 mm HP-NMR tube, pressurized with 5 bar of syngas H₂/CO₂ (1:1), and left at 40 °C for 16 h. After this, the HP-NMR spectra was recorded.

Diffusion-Ordered NMR Spectroscopy Experiments. Diffusion-ordered NMR (DOSY NMR) allows the determination of the translational self-diffusion coefficients (*D*) for these species in acetonitrile solution. Making use of the Stokes–Einstein equation (eq 1), the hydrodynamic radii (*r*_h) for the diffused species can be calculated from the *D* value, represented as⁴²

$$D = \frac{kT}{6\pi\eta r_h} \quad (1)$$

where *k* is the Boltzmann constant, *T* is the temperature, and *η* is the viscosity of the solvent (*η*(CH₃CN) = 0.35 mPa s).

General Procedure for UV–Vis Titrations. Host–guest interactions in solution were studied by UV–vis spectroscopy. Solutions of nanocapsule 4-(BARF)₈ (4.32 × 10^{−7} M) and of the different substrates tested (1.39 × 10^{−5} M) were prepared, using CH₃CN/toluene (1:9) as solvent. An increasing number of substrate equivalents were added to the nanocapsule solution (2 mL in a 1 cm cuvette cell). The host concentration was kept constant. The stoichiometry of the complexes was studied using the method of continuous variations, by adding different ratios of guest solution, in order to add an increasing number of substrate equivalents.

Hydroformylation Catalysis. Hydroformylation experiments were carried out in a stainless-steel autoclave charged with an inset suitable for eight reaction vessels (equipped with teflon mini stirring bars) for performing parallel reactions. Each vial was charged with phosphoramidite ligands (**α**, **β**, **γ**, and **δ**; 0.083 μmol), template Zn-TTP (0.166 μmol) or nanocapsule 4-(BARF)₈ (0.083 μmol), [Rh(acac)(CO)₂] (0.016 μmol), the substrate (83 μmol), and a mixture of toluene/acetonitrile (4:1 v/v). The substrates were filtered through basic aluminum to remove possible peroxide impurities. The solvents were distilled from sodium prior to use. Before starting the

catalysis, the charged autoclave was purged three times with 10 bar of syngas (H_2/CO , 1:1) and then pressurized to 20 bar. After the catalytic reaction, the autoclave was cooled to room temperature if the reaction was carried out at a high temperature, the pressure was reduced to 1.0 bar, and a few drops of tributyl-phosphite were added to each reaction vessel to prevent any further reaction. The reaction mixtures were not filtered over basic aluminum to remove the catalyst residues because filtration may cause retention of the aldehydes, influencing the GC results. The mixtures were diluted with CH_2Cl_2 for GC analysis. The enantiomeric excess was analyzed by GC (Supelco β -dex 225 capillary column). The absolute configuration was determined by comparing the chiral GC traces of the reaction mixture with the those of commercially available enantiopure aldehydes.

■ ASSOCIATED CONTENT

■ Supporting Information

DOSY 2D experiments of $4,4'$ -bpyC4-(BARF)₈, all 1D and 2D NMR spectra, HRMS results, UV-vis experiments, chiral GC data for hydroformylation products, and information and chromatograms (Figures S33–37). This material is available free of charge via the Internet at <http://pubs.acs.org>.

■ AUTHOR INFORMATION

Corresponding Authors

*miquel.costas@udg.edu

*xavi.ribas@udg.edu

*J.N.H.Reek@uva.nl

Notes

The authors declare no competing financial interest.

■ ACKNOWLEDGMENTS

We thank the European Research Council (ERC-2011-StG-277801 to X.R., ERC-2009-StG-239910 to M.C., and ERC-2013-AdG-339782-NAT_CAT to J.N.H.R.), the Spanish MINECO (Consolider-Ingenio CSD2010-00065, INNPLAN-TA project INP-2011-0059-PCT-420000-ACT1, and CTQ2012-32436), and the Catalan DIUE of the Generalitat de Catalunya (2009SGR637 and PhD grant to C.G.S.). X.R. and M.C. are also grateful for ICREA-Acadèmia awards.

■ REFERENCES

- (1) Reetz, M. T. *Angew. Chem., Int. Ed.* **2011**, *50*, 138–174.
- (2) Dang, D.; Wu, P.; He, C.; Xie, Z.; Duan, C. *J. Am. Chem. Soc.* **2010**, *132*, 14321–14323.
- (3) Banerjee, M.; Das, S.; Yoon, M.; Choi, H. J.; Hyun, M. H.; Park, S. M.; Seo, G.; Kim, K. *J. Am. Chem. Soc.* **2009**, *131*, 7524–7525.
- (4) Zhang, Y.; Wang, S.; Enright, G. D.; Breeze, S. R. *J. Am. Chem. Soc.* **1998**, *120*, 9398–9399.
- (5) Stang, P. J.; Olenyuk, B. *Angew. Chem., Int. Ed.* **1996**, *35*, 732–6.
- (6) Jouffroy, M.; Gramage-Doria, R.; Armspach, D.; Sémeril, D.; Oberhauser, W.; Matt, D.; Toupet, L. *Angew. Chem., Int. Ed.* **2014**, *53*, 3937–3940.
- (7) Lee, S. J.; Cho, S.-H.; Mulfort, K. L.; Tiede, D. M.; Hupp, J. T.; Nguyen, S. T. *J. Am. Chem. Soc.* **2008**, *130*, 16828–16829.
- (8) Kuil, M.; Goudriaan, P. E.; van Leeuwen, P. W. N. M.; Reek, J. N. H. *Chem. Commun.* **2006**, 4679–4681.
- (9) Kuil, M.; Goudriaan, P. E.; Kleij, A. W.; Tooke, D. M.; Spek, A. L.; van Leeuwen, P. W. N. M.; Reek, J. N. H. *Dalton Trans.* **2007**, 2311–2320.
- (10) Bellini, R.; Chikkali, S. H.; Berthon-Gelloz, G.; Reek, J. N. H. *Angew. Chem., Int. Ed.* **2011**, *50*, 7342–7345.
- (11) Bellini, R.; Reek, J. N. H. *Chem.—Eur. J.* **2012**, *18*, 7091–7099.
- (12) Bellini, R.; Reek, J. N. H. *Chem.—Eur. J.* **2012**, *18*, 13510–13519.
- (13) Bellini, R.; Reek, J. N. H. *Eur. J. Inorg. Chem.* **2012**, 2012, 4684–4693.
- (14) Gadzikwa, T.; Bellini, R.; Dekker, H. L.; Reek, J. N. H. *J. Am. Chem. Soc.* **2012**, *134*, 2860–2863.
- (15) Yoshizawa, M.; Tamura, M.; Fujita, M. *Science* **2006**, *312*, 251–254.
- (16) Pluth, M. D.; Bergman, R. G.; Raymond, K. N. *Science* **2007**, *316*, 85–88.
- (17) Yoshizawa, M.; Klosterman, J. K.; Fujita, M. *Angew. Chem., Int. Ed.* **2009**, *48*, 3418–3438.
- (18) Pluth, M. D.; Bergman, R. G.; Raymond, K. N. *Acc. Chem. Res.* **2009**, *42*, 1650–1659.
- (19) Kleij, A. W.; Reek, J. N. H. *Chem.—Eur. J.* **2006**, *12*, 4218–4227.
- (20) Pemberton, B. C.; Raghunathan, R.; Volla, S.; Sivaguru, J. *Chem.—Eur. J.* **2012**, *18*, 12178–12190.
- (21) Koblenz, T. S.; Wassenaar, J.; Reek, J. N. H. *Chem. Soc. Rev.* **2008**, *37*, 247–262.
- (22) Raynal, M.; Ballester, P.; Vidal-Ferran, A.; van Leeuwen, P. W. N. M. *Chem. Soc. Rev.* **2014**, *43*, 1734–1787.
- (23) Breiner, B.; Clegg, J. K.; Nitschke, J. R. *Chem. Sci.* **2011**, *2*, 51–56.
- (24) Wiester, M. J.; Ulmann, P. A.; Mirkin, C. A. *Angew. Chem., Int. Ed.* **2011**, *50*, 114–137.
- (25) Leenders, S. H. A. M.; Gramage-Doria, R.; de Bruin, B.; Reek, J. N. H. *Chem. Soc. Rev.* **2015**, *44*, 433–448.
- (26) Brown, C. J.; Bergman, R. G.; Raymond, K. N. *J. Am. Chem. Soc.* **2009**, *131*, 17530–17531.
- (27) Zhao, C.; Sun, Q.-F.; Hart-Cooper, W. M.; DiPasquale, A. G.; Toste, F. D.; Bergman, R. G.; Raymond, K. N. *J. Am. Chem. Soc.* **2013**, *135*, 18802–18805.
- (28) Zhao, C.; Toste, F. D.; Raymond, K. N.; Bergman, R. G. *J. Am. Chem. Soc.* **2014**, *136*, 14409–14412.
- (29) Slagt, V. F.; Reek, J. N. H.; Kamer, P. C. J.; van Leeuwen, P. W. N. M. *Angew. Chem., Int. Ed.* **2001**, *40*, 4271–4274.
- (30) Slagt, V. F.; Kamer, P. C. J.; van Leeuwen, P. W. N. M.; Reek, J. N. H. *J. Am. Chem. Soc.* **2004**, *126*, 1526–1536.
- (31) Kuil, M.; Soltner, T.; van Leeuwen, P. W. N. M.; Reek, J. N. H. *J. Am. Chem. Soc.* **2006**, *128*, 11344–11345.
- (32) Bocokić, V.; Kalkan, A.; Lutz, M.; Spek, A. L.; Gryko, D. T.; Reek, J. N. H. *Nat. Commun.* **2013**, *4*, 2670.
- (33) García-Simón, C.; García-Borrás, M.; Gómez, L.; Parella, T.; Osuna, S.; Juanhuix, J.; Imaz, I.; MasPOCH, D.; Costas, M.; Ribas, X. *Nat. Commun.* **2014**, *5*, 5557.
- (34) O'Sullivan, M. C.; Sprafke, J. K.; Kondratuk, D. V.; Rinfrey, C.; Claridge, T. D. W.; Saywell, A.; Blunt, M. O.; O'Shea, J. N.; Beton, P. H.; Malfois, M.; Anderson, H. L. *Nature* **2011**, *469*, 72–75.
- (35) Pazderski, L. *Magn. Reson. Chem.* **2008**, *46*, S3–S15.
- (36) Kline, M.; Cheatham, S. *Magn. Reson. Chem.* **2003**, *41*, 307–314.
- (37) Franke, R.; Selent, D.; Boerner, A. *Chem. Rev.* **2012**, *112*, 5675–5732.
- (38) Agbossou, F.; Carpentier, J. F.; Mortreux, A. *Chem. Rev.* **1995**, *95*, 2485–2506.
- (39) Dieguez, M.; Pàmies, O.; Claver, C. *Tetrahedron: Asymmetry* **2004**, *15*, 2113–2122.
- (40) Klosin, J.; Landis, C. R. *Acc. Chem. Res.* **2007**, *40*, 1251–1259.
- (41) Chikkali, S. H.; van der Vlugt, J. L.; Reek, J. N. H. *Coord. Chem. Rev.* **2014**, *262*, 1–15.
- (42) Ribas, X.; Dias, J. C.; Morgado, J.; Wurst, K.; Almeida, M.; Parella, T.; Veciana, J.; Rovira, C. *Angew. Chem., Int. Ed.* **2004**, *43*, 4049–4052.